HHS Public Access

Author manuscript

Cell Rep. Author manuscript; available in PMC 2016 August 31.

Published in final edited form as:

Cell Rep. 2016 August 16; 16(7): 1861–1873. doi:10.1016/j.celrep.2016.07.025.

Dis3l2-Mediated Decay Is a Quality Control Pathway for Noncoding RNAs

Mehdi Pirouz[1,2], **Peng Du**[1,2], **Marzia Munafò**[1], and **Richard I. Gregory**[1,2,3,4,5]

[1]Stem Cell Program, Division of Hematology/Oncology, Boston Children's Hospital, Boston, MA 02115

[2]Department of Biological Chemistry and Molecular Pharmacology, Harvard Medical School, Boston MA 02115

[3]Department of Pediatrics, Harvard Medical School, Boston MA 02115

[4]Harvard Stem Cell Institute, Boston MA 02115

SUMMARY

Mutations in the 3′-5′ exonuclease DIS3L2 are associated with Perlman syndrome and hypersusceptibility to Wilms' tumorigenesis. Previously, we found that Dis3l2 specifically recognizes and degrades uridylated pre-let-7 microRNA. However, the widespread relevance of Dis3l2-mediated decay of uridylated substrates remains unknown. Here we applied an unbiased RNA immunoprecipitation strategy to identify Dis3l2 targets in mouse embryonic stem cells. The disease-associated long noncoding RNA (lncRNA) Rmrp, 7SL, as well as several other Pol III-transcribed noncoding RNAs (ncRNAs) were among the most highly enriched Dis3l2-bound RNAs. 3′-uridylated Rmrp, 7SL, and snRNA species were highly stabilized in the cytoplasm of Dis3l2-depleted cells. Deep sequencing analysis of Rmrp 3′ ends revealed extensive oligouridylation mainly on transcripts with imprecise ends. We implicate the TUTases Zcchc6/11 in the uridylation of these ncRNAs, and biochemical reconstitution assays demonstrate the sufficiency of TUTase-Dis3l2 for Rmrp decay. This establishes Dis3l2-Mediated Decay (DMD) as a quality control pathway that eliminates aberrant ncRNAs.

eTOC

DIS3L2 is mutated in Perlman syndrome and Wilms tumors but substrates of this exoribonuclease remain to be examined. Pirouz et al. systematically identify noncoding RNAs (ncRNAs) as the

[5]Corresponding author: Richard I. Gregory, Phone: (617) 919-2273, Fax: (617) 730-0748, rgregory@enders.tch.harvard.edu.

Accession Numbers

GSE84107

AUTHOR CONTRIBUTIONS

M.P. performed all experiments with help from M.M. P.D. generated the Dis3l2 knockout ESCs and performed all the bioinfomatics analysis. M.P. and R.I.G. designed all experiments, analyzed data, and wrote the manuscript with input from M.M. and P.D.

major targets of Dis3l2 in mouse ESCs. Dis3l2-mediated decay serves as a quality control pathway that eliminates ncRNAs with aberrant 3′ ends.

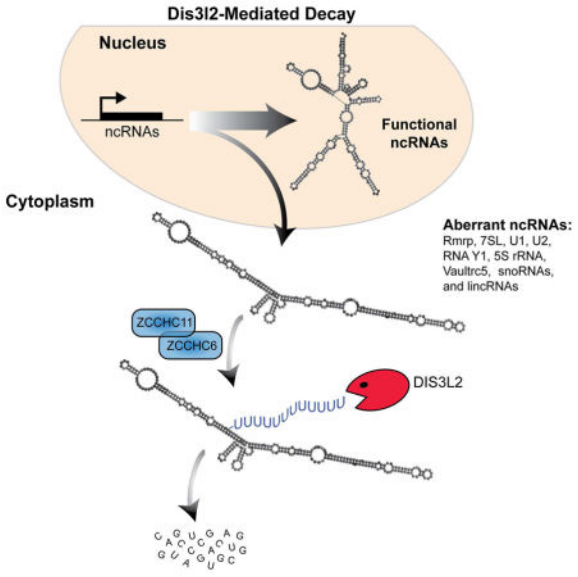

Keywords

Dis3l2; Zcchc6; Zcchc11; Uridylation; TUTase; Rmrp; 7SL; snRNA; lncRNA

INTRODUCTION

Dis3l2 is a mammalian exosome-independent homolog of yeast Dis3, with 3′-5′ exoribonuclease activity. We, and others, previously identified Dis3l2 as the exonuclease that functions in the Lin28-mediated repression and degradation of let-7 microRNAs (miRNAs) in mouse embryonic stem cells (mESCs) (Chang et al., 2013; Ustianenko et al., 2013). Lin28 recruits the Terminal Uridylyl Transferases (TUTases) Zcchc6 (TUT7) and Zcchc11 (TUT4) to target precursor let-7 (pre-let-7) RNAs for degradation by Dis3l2 (Hagan et al., 2009; Heo et al., 2009; Lin and Gregory, 2015; Thornton et al., 2012). Biochemical and structural studies revealed that a stretch of oligo-uridylation (~12 Uridines) at the 3′ end of transcripts serves as the recognition signal for Dis3l2 to bind and degrade substrate RNAs (Chang et al., 2013; Faehnle et al., 2014). Mutations in *DIS3L2* are involved in the Perlman overgrowth and Wilms' tumor predisposition syndrome (Astuti et al., 2012). Moreover, *DIS3L2* mutations or deletions have been reported in sporadic Wilms' tumors (Astuti et al., 2012; Morris et al., 2013; Wegert et al., 2015). Despite these strong links between DIS3L2 deficiency and human disease, very little is known about the role of Dis3l2 in RNA regulation and specifically the identity of its direct targets has so far remained elusive. Although deep sequencing analysis has shown changes in mRNA expression in Dis3l2-depleted human cells (Lubas et al., 2013), it is not clear whether this reflects a direct and/or indirect consequence of Dis3l2 loss. Indeed, Dis3l2 has been largely eliminated as a possible regulator of uridylated histone messenger RNAs (mRNAs) as well as other mRNAs with short U-tails (Lim et al., 2014; Slevin et al., 2014). Dis3l2 has been recently implicated in

apoptosis-induced mRNA degradation (Thomas et al., 2015), as well as target RNA-directed miRNA degradation (TDMD) (Haas et al., 2016). So far, a systematic identification of Dis3l2 direct targets has not been performed and the repertoire of regulated RNAs remains unknown.

The RNA Polymerase (Pol) III transcriptome (also called class III genes) includes a growing list of genes. Originally, RNA Pol III was considered specialized for transcription of highly abundant transfer RNAs (tRNAs) and 5S ribosomal RNA (5S rRNA) species, which are engaged in protein synthesis. However, over the past several years, RNA Pol III has been reported to be responsible for transcription of many other noncoding RNAs (ncRNAs). These include Rmrp (RNase MRP), Rpph1 (RNase P), U6 small nuclear RNA (snRNA), 7SL, 7SK, BC200, Vault, SINE (short interspersed repeated DNA elements)-encoded RNAs, as well as small nucleolar (sno) RNAs, and some miRNAs [for review see (Dieci et al., 2007)]. Pol III-mediated transcription can be launched through a variety of internal promoter elements, box A and box B, or box C (for 5S rRNA), as well as upstream TATA (like)-box, proximal and/or distal sequence elements or their combinations (for 7SK, Rmrp and Rpph1). In contrast, eukaryotic RNA Pol III terminates transcription uniquely at a short stretch of Thymidine (oligo-T) residues on the non-templated strand of DNA and following synthesis of a short uridine stretch (U-stretch) on nascent RNA (Bogenhagen and Brown, 1981; Matsuzaki et al., 1994). This oligo-T transcription termination signal serves both as recognition and pause signal (Arimbasseri and Maraia, 2015; Braglia et al., 2005; Nielsen et al., 2013; Orioli et al., 2012), which allows the release of nascent RNA and polymerase from DNA due to the low stability of oligo (dA:rU) DNA:RNA duplex (Martin and Tinoco, 1980). Efficient termination can be achieved with the minimal length of 4, or 5 Us at the 3′ end of the transcripts in vertebrates and yeast, respectively (Allison and Hall, 1985; Braglia et al., 2005). RNA Pol III termination results in the incorporation of a variable length oligo-U tract at the 3′ end of the Pol III-primary transcripts. For tRNAs these 3′ trailers are removed post-transcriptionally by RNase Z that together with other exonucleases generate the 3′ end of the mature tRNA (Maraia and Lamichhane, 2011). While extended transcription beyond termination signal may provide developmental advantages (Orioli et al., 2011), failure in trailer trimming can also be implicated in disease development (Haack et al., 2013). Moreover, upon Pol III-induced read-through of the genomic DNA, the unprocessed 3′ oligo-U tract may hybridize with internal sequences and interfere with proper folding and abrogate the function of Pol III transcripts.

Rmrp is a highly conserved long noncoding RNA (lncRNA) with endoribonuclease activity (Hsieh et al., 1990). Historically, Rmrp was described as a “Ribozyme” i.e. an RNA molecule with enzymatic activity (Kruger et al., 1982). It forms a ribonucleoprotein complex that is well characterized in different organisms (Fagerlund et al., 2015; Gold et al., 1989; Lygerou et al., 1994). Recessive mutations in human *RMRP* cause cartilage-hair hypoplasia (CHH) (Ridanpaa et al., 2001) with a wide range of manifestations including short stature, anemia, immune deficiency, impaired spermatogenesis, increased rate of skin cancer and metaphyseal dysplasia (Makitie, 1992; Makitie et al., 1999; Makitie et al., 2001; Trojak et al., 1981). Studies in yeast models suggested that Rmrp is involved in pre-ribosomal RNA (pre-rRNA) processing (Chu et al., 1994) and 5′ UTR cleavage of Cyclin B2 mRNA (Cai et al., 2002; Gill et al., 2004); however, the exact role of Rmrp in vertebrates remains to be

elucidated (Huang et al., 2015). An increasing number of RMRP mutations are reported that cause CHH in various populations (Bonafe et al., 2005; Cherkaoui Jaouad et al., 2015; Thiel et al., 2007). RMRP is a highly structured RNA, in which mutation-induced perturbations throughout most of 265 nucleotides of human transcript are associated with different aspects of CHH. This highlights the significance of retaining intact transcripts in cells and suggests a demand for, as yet unknown, Rmrp-associated quality control pathway(s).

Here, we performed a systematic analysis of RNAs that associate with a catalytically inactive version of Dis3l2 isolated from Dis3l2-deficient mouse ESCs. This revealed Dis3l2 targets to be highly enriched for RNA Pol III-transcribed ncRNAs including Rmrp, 7SL, and several others. Using CRISPR/Cas9 knockout and RNAi-mediated knockdown approaches we find that Dis3l2 loss-of-function causes the stabilization of 3′-uridylated Rmrp, 7SL, and snRNAs species in the cell cytoplasm. Deep sequencing analysis of Rmrp 3′ ends from Dis3l2 knockout cells revealed extensive oligouridylation mainly on Rmrp transcripts with imprecise terminated ends supporting that Dis3l2 normally safeguards the elimination of these aberrant Rmrp transcripts. We identify the paralogous TUTases Zcchc6 and Zcchc11 to be responsible for ncRNA uridylation and reconstitute the TUTase-Dis3l2 decay *in vitro* using recombinant proteins. Unlike mRNA quality control pathways including nonsense-mediated decay (NMD) that require mRNA translation, we identify Dis3l2-Mediated Decay (DMD) as a quality control pathway that eliminates aberrant ncRNAs.

RESULTS

Global identification of Dis3l2 target RNAs

To explore the widespread relevance of Dis3l2 in the control of RNA metabolism we established a biochemical method for the unbiased identification of Dis3l2 targets. This involved the generation of Dis3l2 knockout ESCs (to stabilize labile Dis3l2 substrates) and the expression of a catalytically inactive Dis3l2 that retained its RNA-binding capability (to identify direct Dis3l2 substrate RNAs). We used the CRISPR/Cas9 editing system to generate Dis3l2 knockout mouse ESCs (Figure S1A). Deletion of Dis3l2 genomic DNA and subsequently loss of protein expression in knockout ESCs was confirmed by PCR (Figure S1B) and western blot analysis (Figure 1A, and Figure S1C), respectively. Dis3l2$^{-/-}$ ESCs were transfected with a plasmid for expression of a catalytic mutant FLAG-tagged Dis3l2 (D389N substitution) that we previously showed can bind but not degrade RNA (Chang et al., 2013). Moreover, the relative expression level and subcellular localization of the catalytic mutant Dis3l2 is comparable to the wild-type protein when ectopically expressed (Chang et al., 2013). Potential Dis3l2 substrates were immunoprecipitated (IP) using anti-FLAG antibody (Figure 1B). As a negative control, cells were transfected in parallel with FLAG-empty vector (Mock). The precipitated Dis3l2 ribonucleoprotein complexes were reverse cross-linked and RNA was isolated and sequenced (RIP-Seq, Supplemental Table 1). A scatter plot of the RIP-Seq data revealed a significant enrichment of several transcripts in mutant FLAG-Dis3l2 IP (Figure 1C). Among the highly enriched transcripts were the lncRNA components of the two related ribozymes: RNase MRP (Rmrp) and RNase P (Rpph1) as well as the two Rpph1 pseudogenes, Rprl2 and Rprl3. (Figure 1C, D). Rmrp and Rpph1 are two ubiquitously expressed conserved RNA Pol III-transcribed lncRNAs with

enzymatic activity and are highly expressed in various cell types. In contrast to Rmrp and Rpph1, other transcripts with even higher abundance, Malat1 and Lars2, were not enriched in Dis3l2-RIP (Figure 1C, E), supporting the specificity of these interactions. Independent immunoprecipitation of mutant FLAG-Dis3l2 followed by quantitative reverse transcriptase-PCR (qRT-PCR) showed a significant enrichment of these two lncRNAs, especially Rmrp (Figure 1E). Finally, qRT-PCR analysis of immunoprecipitated RNA samples (Figure 1F) showed a strong enrichment of Rmrp in mutant FLAG-Dis3l2 but not wild type FLAG-Dis3l2 IPs (Figure 1G).

Uridylated Rmrp accumulates in the cytoplasm of Dis3l2-depleted ESCs

We reasoned that if Dis3l2 is involved in the 3′-5′ decay of its substrates, uridylated species of Rmrp and Rpph1 should accumulate in Dis3l2-deficient cells. To quantify the relative uridylation of different transcripts, cDNA synthesis was performed using oligo-$dA_{(12)}$ primers that enriched specifically for uridylated RNA species. While the relative expression of Rmrp measured by qRT-PCR analysis of random hexamer-primed cDNA was only increased modestly (Figure 2A), a marked increase in relative Rmrp and pre-let-7g uridylation was observed in Dis3l2 knockout cells compared to heterozygous and wild-type ESC controls (Figure 2B). This suggests a posttranscriptional regulation of Rmrp and pre-let-7g. Neither relative uridylation nor expression of Rpph1 and Sox2 changed in Dis3l2 knockout ESCs. To further confirm these findings we knocked down Dis3l2 in ESCs using shRNA and measured relative expression and uridylation levels (Figure S2). Consistent with the results in knockout cells, the level of uridylated Rmrp, but not Rpph1, increased in a dose-dependent manner in the shDis3l2 stable knockdown ESCs (Figure S2A–C). Transient knockdown of Dis3l2 using siRNA showed a similar effect on Rmrp uridylation (Figure S2D–F). Thus, the level of uridylated Rmrp is increased substantially in the absence of Dis3l2. Dis3l2 rescue experiments were performed by transfecting wild type FLAG-Dis3l2 expression plasmids in Dis3l2-knockout ECSs. Western blot analysis showed the expression of Dis3l2 in knockout cells similar to the endogenous levels in wild type ESCs (Figure 2C). qRT-PCR analysis showed a dramatic accumulation of uridylated Rmrp and pre-let-7g in Dis3l2 knockout ESCs that was significantly reduced upon transient transfection of Dis3l2 (Figure 2D).

Rmrp is a mostly nuclear RNA (Jacobson et al., 1995), whereas Dis3l2 is mainly localized to the cytoplasm (Chang et al., 2013; Lubas et al., 2013; Ustianenko et al., 2013). It is therefore anticipated that uridylated Rmrp transcripts should accumulate in the cytoplasm of Dis3l2-deficient cells. To test this, cell fractionation was performed on two control ESC lines as well as two Dis3l2 knockout cells and nuclear and cytoplasmic RNAs were analyzed by qRT-PCR. As expected Gapdh mRNA was predominantly detected in cytoplasmic fractions, whereas U6 and Rmrp were mainly detected in the nuclear RNA fraction (Figure 2E). Similar to the pre-let-7g positive control, relative uridylation of Rmrp was consistently increased up to 100-fold in the cytoplasmic fraction of two independent Dis3l2 knockout ESC lines (Figure 2F). Northern blot analysis performed on cytoplasmic RNA samples provided further support for specific accumulation of an extended, slower migrating, Rmrp transcript (but not 7SK or Rpph1 RNAs) in only Dis3l2-deficient cells (Figure 2G).

Rmrp uridylation occurs on transcripts with imprecise 3′ ends

Next we asked whether the Rmrp tails that Dis3l2 recognizes are indeed poly-U oligonucleotides at 3′ end of Rmrp. To answer this, we first tested if oligo-$dA_{(12)}$ primers could recognize oligo-U stretches at 3′ end; cDNA preparation from cytoplasmic RNAs by oligo-$dA_{(12)}$ and PCR amplification of cDNAs using Rmrp specific primers and gel electrophoresis revealed a single band of less than 300 bp PCR product in Dis3l2 knockout samples, which was absent in control cells (Figure S3A). Sanger sequencing confirmed the identity of this PCR product to be corresponding to the full length Rmrp (data not shown). Next, we used an oligo-$dA_{(12)}$ adaptor oligonucleotide to synthesize cDNA from cytoplasmic RNA of ESCs, and then performed PCR with Rmrp- and adaptor-specific primers (Figure S3B). Similarly, gel electrophoresis resolved a single expected band of ~100 bp PCR product solely in Dis3l2 knockout samples, thereby supporting that uridylation occurred at the 3′ end of Rmrp.

To determine the sequence identity of Rmrp tail in Dis3l2 knockout ESCs at single nucleotide resolution, we performed Rapid Amplification of cDNA Ends from circularized RNA samples (cRACE). To this end, cytoplasmic RNA from Dis3l2 knockout ESCs, as well as input, and mutant Dis3l2-IP RNA samples were isolated and then circularized using T4 RNA ligase. Reverse transcription (RT) of RNA transcripts with Rmrp-specific primers followed by PCR reaction using divergent forward and reverse Rmrp-specific primers yielded a chimeric PCR product that specifically originated from circularized RNAs and contained the 3′ tail sequence (Figure 3A). Sanger sequencing of this PCR product revealed Rmrp containing oligo-U tails of 5 and 9 nucleotides long in cytoplasmic Dis3l2 knockout samples (Figure S3C). More comprehensively, Mi-Seq analysis of chimeric PCR products from input and IP samples identified the oligo-U tails at 3′ end of Rmrp that were distinguishable from Rmrp genomic sequence (Figure 3B). In IP samples, Rmrp tails of up to 26 continuous Uridines were detected, with a peak length distribution of 10–12 nucleotides. Intriguingly this peak U-tail length is highly consistent with the structural basis for Dis3l2 interaction with the oligo-U tail of pre-let-7 (Faehnle et al., 2014) (Figure 3B). Moreover, the length and proportion of Rmrp U-tails were significantly higher in IP samples compared to input, suggesting specific enrichment of these tails in mutant Dis3l2-IP. A closer inspection of this sequencing data intriguingly revealed that almost all the U-tails of both input and IP transcripts occurred 2 nucleotides after annotated 3′ end of Rmrp (Figure 3C). This raised the possibility that Rmrp uridylation might occur mainly on transcripts containing extra nucleotides at their 3′ ends perhaps caused by inaccurate transcription termination. This observation promoted us to examine the exact 3′ end of Rmrp in both input and IP RNA samples. Surprisingly, only a small fraction of Rmrp species in input ended with the annotated Cytosine nucleotide (5.7%), whereas, more than 85% of Rmrp transcripts had one nucleotide less and ended with Adenosine (Figure 3D). This indicates that Rmrp transcripts ending in this Adenosine are the predominant species in mouse ESCs and this might represent the actual 3′ end of mouse Rmrp in ESCs. In contrast, more than 97% of U-tailed Rmrp species in IP samples were extended by three nucleotides than the newly established 3′ end (Figure 3D). Moreover, *in silico* RNA-fold analysis revealed that an additional CAC and 5 or more uridines at the 3′ end could dramatically alter the predicted Rmrp secondary structure (Figure S3D). Thus, mutant Dis3l2 enriches for Rmrp

species with U-tails and this uridylation occurs mainly on inaccurately terminated Rmrp transcripts. Altogether these data indicate that Dis3l2 might be part of a quality control pathway responsible for ensuring the fidelity of the Rmrp 3′ end.

Zcchc6 and Zcchc11 are TUTases that trigger Dis3l2-mediated Rmrp decay

Zcchc6 and Zcchc11 are the two TUTase enzymes responsible for uridylation of pre-let-7 miRNAs. We asked if these enzymes are also involved in terminal uridylation of Rmrp. Individual, and simultaneous knockdown of Zcchc6 and Zcchc11 led to a reduction in the levels of Rmrp and pre-let-7g uridylation (Figure 4A, B). We examined whether recombinant Zcchc11 (expressed and purified from bacteria) could directly uridylate Rmrp species with additional CAC at the 3′ end. *In vitro* transcribed $Rmrp^{+CAC}$ was incubated with increasing amounts of recombinant Zcchc11 in the presence of radiolabeled UTP. This showed that Zcchc11 is sufficient to uridylate Rmrp in a dose-dependent manner (Figure 4C). Next, we set out to reconstitute uridylation-dependent Dis3l2-mediated Rmrp decay *in vitro. In vitro* transcribed radiolabeled $Rmrp^{+CAC}$ RNAs were subjected to Dis3l2 degradation (using recombinant Dis3l2 expressed and purified from bacteria) in the presence or absence of recombinant Zcchc11. Indeed, Dis3l2-mediated Rmrp degradation was found to be dependent on Zchcc11 thereby demonstrating the TUTase dependency of Dis3l2-mediated decay and furthermore revealing the sufficiency of these two proteins for the targeted degradation of Rmrp *in vitro* (Figure 4D). Altogether, our results identify TUTase-dependent Dis3l2-Mediated Decay (DMD) as a quality control pathway that ensures the fidelity of the 3′ end of Rmrp (Figure 4E).

Dis3l2-Mediated Decay (DMD) regulates ncRNAs

Considering that the most enriched RNAs identified in FLAG-mutant Dis3l2 were long noncoding RNAs and that Dis3l2-depletion had no effect on any of the mRNAs we tested (Figure 1C and data not shown), we next asked whether DMD might be more generally relevant to certain ncRNAs. RIP-Sequencing reads were initially mapped to a database biased towards the coding portion of the genome (UCSC), which essentially overlooked the noncoding component of the transcriptome (Figure 1C). Therefore, we re-examined RIP-Seq data and mapped the sequencing reads to the annotated noncoding transcripts (ENSEMBL). Interestingly, this analysis revealed the most enriched RNAs in FLAG-mutant Dis3l2 samples to be ncRNAs (Figure 5A, Supplemental Table 2). This predominantly included RNA Pol III-transcribed lncRNAs including 7SL (the RNA component of SRP [Signal Recognition Particle]), Rmrp and Rpph1 (as we initially found), Vaultrc5, several snoRNAs, RNA Y1, 5S rRNA, as well as RNA Pol II-transcribed noncoding U1 and U2 snRNA, and several other uncharacterized ncRNAs (Supplemental Table 2). We next tested whether similar to our findings on Rmrp, Dis3l2-TUTase axis might also be involved in the regulation of other ncRNAs identified, including the most highly enriched transcript, 7SL. RIP-qPCR analysis showed that 7SL, and especially uridylated 7SL, is associated with FLAG-mutant Dis3l2 (Figure 5B). Increased uridylation of 7SL was observed in two $Dis3l2^{-/-}$ ESC lines by qRT-PCR analysis of total and cytoplasmic RNA fractions (Figure 5C and D) as well as by Northern blot analysis (Figure 5E). We adapted the cRACE protocol for 7SL and examined 3′ end of cytoplasmic 7SL in $Dis3l2^{-/-}$ ESCs. Sanger sequencing of cRACE chimeric PCR products showed the presence of U-tails in most (12 out of 15) of the

analyzed clones. Occasionally, these tails occurred in clones with truncated 3′ ends (Figure 5F). Moreover, transient knockdown of Zcchc6, Zcchc11, or both led to a substantial decrease in relative uridylation of 7SL in Dis3l2 knockout ESCs (Figure 5G). Finally, re-expression of Dis3l2 in knockout cells could rescue relative uridylation of 7SL to a level similar to that of wild-type cells (Figure 5H). Since the specific U1 and U2 isoforms, U1a1 and U2–10, respectively, were among the most highly enriched RNAs in the Dis3l2 IP (Supplemental Table 2) we next examined the role of Dis3l2 in regulation of U1 and U2 snRNAs. qRT-PCR analysis showed that, although the total level of these two snRNAs was unchanged in the Dis3l2 knockout cells, the level of uridylated U1 and U2 was elevated in both total RNA as well as in cytoplasmic RNA fractions from Dis3l2 knockout ESCs compared to wild-type cells (Figure 6A–C). We next performed 3′-ligation RACE analysis of the U1 and U2 snRNAs in FLAG-mutant Dis3l2 IP samples (Figure 6D). Sanger sequencing of the PCR products resulting from amplification of 3′ end junctions revealed several clones with U-rich tails in both U1 (Figure 6E) and U2 (Figure 6F) Dis3l2-IP samples. Particularly, the tails occurred on U1 and U2 with extended 3′ sequences implying that DMD targets snRNAs with imprecise 3′ ends as part of a quality control pathway for a set of ncRNAs.

DISCUSSION

Previously, we identified Dis3l2 as the 3′-5′ exonuclease responsible for recognition and degradation of uridylated pre-let-7 miRNAs (Chang et al., 2013). Accordingly, an oligo-U tail is necessary and sufficient to target Dis3l2 binding and exonucleolytic activity (Chang et al., 2013; Faehnle et al., 2014). Given that oligouridylation has been implicated in the metabolism of other RNAs, and that Dis3l2 is expressed in cells that do not co-express Lin28, it is likely that Dis3l2 has additional substrates other than pre-let-7. So far, an unbiased identification of Dis3l2 substrate RNAs has proven to be challenging since these labile RNAs are expected to be difficult to detect in steady state RNA samples. Furthermore, sequencing RNA samples of Dis3l2-depleted cells is likely to uncover many indirect changes in RNA expression. To address this, we developed an innovative strategy to isolate RNAs that are physically associated with Dis3l2. This involved expressing a catalytic mutant version of FLAG-Dis3l2 in Dis3l2-knockout ESCs and performing FLAG-immunopurification of Dis3l2-containing ribonucleoprotein complexes from UV-crosslinked cells. This approach both stabilizes decay substrates (by Dis3l2 deletion) and enriches for direct Dis3l2 targets (by isolating Dis3l2-bound RNAs).

Using this strategy we discovered that the majority of Dis3l2-bound RNA species are ncRNAs that are transcribed by RNA Pol III (Figure 1C, 5A). Two of the most enriched transcripts in Dis3l2-IP were the lncRNA components of RNase MRP and RNase P (Rmrp and Rpph1, respectively) and Rpph1 pseudogenes. Analysis of relative uridylation of Rmrp and Rpph1 proved that Rmrp (but not Rpph1) is a true substrate of Dis3l2 because: 1) Rmrp uridylation is highly stabilized in Dis3l2-depleted cells. 2) Uridylated Rmrp is mostly localized to cytoplasmic fraction where Dis3l2 is also normally located. 3) Ectopic re-expression of Dis3l2 in knockout ESCs significantly decreases Rmrp uridylation. 4) Deep sequencing analysis revealed oligo-uridylation of Rmrp 3′ ends. Interestingly, the peak length of this U-tail is ~12 nucleotides that is highly consistent with previous biochemical

and structural work for Dis3l2 substrate recognition (Chang et al., 2013; Faehnle et al., 2014; Ustianenko et al., 2013). 5) The uridylation-dependent Dis3l2-Mediated Decay of Rmrp could be recapitulated *in vitro* using purified recombinant proteins.

Despite this evidence that Rmrp is a *bona fide* direct target of Dis3l2, it is notable that the steady state levels of Rmrp are not appreciably altered by Dis3l2-depletion. Intriguingly however, our sequencing analysis of Rmrp 3′ ends revealed that the U-tail is specifically added to Rmrp species containing an additional three nucleotides downstream of the normal 3′ end of the Rmrp RNA. These extra (CAC) nucleotides are encoded by the genome and lead us to propose that Dis3l2 serves as a quality control mechanism for the specific decay of aberrant (and possibly dis-functional) Rmrp transcripts with an extended 3′ end. 3′ terminal modification was previously reported for a subset of human RMRP, where oligoadenylation occurred on extended RMRP species with few uridines (Goldfarb and Cech, 2013), further implying post-transcriptional regulation of RMRP. That Dis3l2 degrades only mutant forms of Rmrp helps distinguish this from a general decay pathway controlling Rmrp expression or a biogenesis pathway requiring Dis3l2 for Rmrp 3′ end maturation since these should impact all Rmrp transcripts and have a more dramatic effect on overall Rmrp expression. Interestingly, *RMRP* is itself a disease-associated gene that is mutated in Cartilage-Hair Hypoplasia (CHH), an autosomal recessive disorder characterized by disproportionate short stature and multiple other developmental phenotypes (Ridanpaa et al., 2001). It will be of interest to examine the relationship between DIS3L2 and RMRP in the context of human disease and their opposing roles in human fetal growth.

While quality control pathways are well characterized for coding mRNAs (Garneau et al., 2007), tRNAs (Hopper and Huang, 2015; Kadaba et al., 2006; Vanacova et al., 2005) and rRNAs (Dez et al., 2006; LaRiviere et al., 2006), far less is known about the existence of such mechanisms for other ncRNAs. Quality control mechanisms have been proposed for truncated (Ishikawa et al., 2014) or mutant forms of U1 snRNA (Shukla and Parker, 2014) and 7SL in yeast (Leung et al., 2014) to eliminate aberrant transcripts. Defective U1 snRNAs can be degraded by both 3′-5′ exonuclease Rrp6 and decapping and Xrn1-mediated decay (Shukla and Parker, 2014); however EXOSC10, the human homolog of Rrp6, is dispensable for U1 quality control suggesting separate mechanisms in higher eukaryotes (Shukla and Parker, 2014). In addition, in yeast, Trf4–Air1/2–Mtr4 polyadenylation complex (TRAMP) serves as a nuclear quality control mechanism for noncoding RNA (LaCava et al., 2005). It targets a wide variety of RNAs by addition of 4–5 adenosine residues and marks them for degradation by the nuclear exosome [reviewed in (Wolin et al., 2012)]. TRAMP polyadenylates 3′ end of aberrant 23S rRNA intermediates, truncated 5S rRNAs, 7SL and some tRNAs. By contrast, such 3′ aberrant RNAs that accumulate in yeast upon TRAMP/exosome depletion (including 7SL) are not found in mammals, thus suggesting different pathways in metazoans. Particularly, in line with increased repertoire and complexity of ncRNA genome in evolution (Kapusta and Feschotte, 2014; Mattick, 2011; Rinn and Chang, 2012), there is a special demand for ncRNA-specific quality control pathway(s) in mammals. We extend our findings on Rmrp and examine the role of Dis3l2 in ncRNA regulation more generally. This revealed a strong enrichment for transcripts that are transcribed by RNA Pol III. RNA Pol III nascent transcripts harbor additional Uridine residues at their 3′ end, which might make them favored substrates for

further uridylation by TUTase. Also of relevance, it was shown that recombinant Zcchc11 (TUT4) displays greater *in vitro* TUTase activity towards substrate RNAs without- or with short A-tails compared to longer poly-A-tail containing RNAs (Lim et al., 2014). This likely helps explain the involvement of Zcchc6 and Zcchc11 in the uridylation of Rmrp, and 7SL and the specificity of Dis3l2 for Pol III transcripts and certain non-polyadenylated Pol II transcripts including snRNAs. Zcchc6 and Zcch11 TUTases are localized mainly in the cytoplasm and are therefore physically sequestered from Rmrp. Aberrant Rmrp species must be transfered to the cytoplasm by a yet to be determined export mechanism. This differential subcellular localization may confer TUTase specificity towards those exported Rmrp molecules. In line with this, It has been shown that unlike wild-type Rmrp that is retained in the nucleus when microinjected into rat kidney cells, mutant Rmrp RNA is exported to the cytoplasm, thereby further highlighting the importance of both intact sequence and proper localization for Rmrp function(Jacobson et al., 1995). Although we found a robust interaction between Dis3l2 and lincRNA ribozyme Rpph1, we did not find evidence for Rpph1 uridylation in Dis3l2 knockout cells. Further investigation is required to elucidate biological significance of Dis3l2-Rpph1 interaction. One possibility is that Dis3l2 and Rpph1 form a ribonucleoprotein complex, where the exonuclease activity of Dis3l2 and endonucleolytic activity of Rpph1 are coupled for tRNA maturation and/or decay.

Our unbiased identification and characterization of Dis3l2 substrate RNAs uncovers a heretofore unknown ncRNA quality control pathway and paves the way for future studies aimed at elucidating the particular pathological RNAs and mechanisms associated with Dis3l2 deficiency during fetal development and cancer, including Wilms' tumors.

EXPERIMENTAL PROCEDURES

Cell Culture

TC1 mouse embryonic stem cells (ESCs) were maintained as previously described (Pirouz et al., 2015). Briefly, ESCs were adapted to gelatin cultures and fed with KO-DMEM (Gibco) supplemented with 15% Stem Cell-Qualified Fetal Bovine Serum (FBS, Gemini), L-glutamine (2 nM, gibco), HEPES (20 mM, gibco) sodium pyruvate (1 mM, gibco), non-essential amino acids (0.1 mM each, gibco), 2-mercaptoethanol (100 mM, Sigma), penicillin/streptomycin (10^4 U/ml, gibco), and mLIF (10^3 U/ml, Gemini).

Transfections

For rescue experiments, 1 μg wild type Dis3l2 expressing vectors or empty vectors (as mock) were reverse transfected by Lipofectamine 2000 (Invitrogen) into ESCs. Cells were harvested 48–72 hour post-transfection and analyzed by western blotting or qRT-PCR. Dis3l2 stable knockdown ESCs (shDis3l2 lines) were generated previously (Chang et al., 2013). For transient knockdown experiments, following ON-TARGET plus siRNAs (all Dharmacon) were used: Control siRNA pool (D-001810-10), siDis3l2 pool (L-054755-01), siZcchc6 (L-056770-01), and siZcchc11 pool (L-065226-00). Reverse transfections were performed using siRNAs and Lipofectamine RNAiMax (Invitrogen) complexes prepared in Opti-MEM (Gibco). Cells were harvested for analysis 48–72 hours after transfection.

CRISPR/Cas9-mediated editing of Dis3l2 locus

Dis3l2-specific guide RNAs (Figure S1) were designed (http://crispr.mit.edu/) and cloned into px330 vectors expressing wild type Cas9 (Addgene) and used to transect TC1 ESCs. The complete procedure is explained in the Supplemental Text.

RNA immunoprecipitation and sequencing

ESCs were first transfected with either FLAG-wild type Dis3l2, FLAG-mutant Dis3l2, or empty pFLAG-CMV2 (as mock) vectors (Chang et al., 2013). 48 hours after transfection, cells were washed twice with PBS and UV-crosslinked at 400 Joules/cm^2 energy. Crosslinked cells were lysed in 1 ml protein lysis buffer supplemented with Complete EDTA-free protease inhibitor cocktail (Roche) and 400 units RNaseOUT (Invitrogen) and then treated with RQ1 DNase for 30 minutes at 37 °C. Lysates were centrifuged at 12000g and the supernatants were collected. 1% of the lysates were set aside as inputs. For immunoprecipitation (IP) of FLAG-tagged Dis3l2, anti-FLAG M2 Affinity Gel beads (Sigma) were washed three times in CLIP buffer (0.1% SDS, 0.5% NP-40 in 1x Mg/Ca-free PBS). Lysates from an equivalent of around 3×10^7 cells were used for each IP reaction and incubated with 50 μl pre-washed beads for 2–3 hours rotating at 4 °C. Beads were then centrifuged at 2500 g for 3 minutes and washed 4 times with cold CLIP buffer and subsequently 4 times with high-salt wash buffer (0.1% SDS, 0.5% NP-40 in 5X Mg/Ca-free PBS) at room temperature. After the last wash, 10% of the immunoprecipitates were set aside to check IP efficiency by western blotting. The rest of the beads were re-suspended with protein lysis buffer containing 100 μg Proteinase K (Ambion) and incubated at 45 °C for 45 minutes for reverse crosslinking, and then subjected to RNA extraction. Around 100 ng of immunoprecipitated RNA from inputs or IP samples were used for cDNA synthesis using random hexamers or oligo-dA oligonucleotides, or alternatively for RNA library preparation. RNA library preparation was performed on IP samples and RiboMinus-(Ambion) selected inputs following TruSeq Standard mRNA Sample Preparation Guide (Illumina). Libraries were subjected to Illumina high-throughput sequencing.

Amplification of Rmrp 3′ end and cRACE

Cytoplasmic RNA samples from ESCs were reverse transcribed using oligo-$dA_{(12)}$ adapters and amplified with Rmrp-specific forward and adapter-specific primers (Supplemental Table 3). PCR products were resolved in 2% agarose gels and visualized. RNA samples of cytoplasmic (2 μg) or FLAG-mutant Dis3l2 IP (100 ng) were circularized with 1 μl T4 RNA ligase I (NEB), 10 mM ATP (NEB), 10% PEG 8000, in 1X T4 RNA ligase buffer for 2 hours at 37 °C and then the ligase was inactivated for 5 minutes at 95 °C. Circularized RNAs were precipitated with acidic phenol-chloroform (Ambion) and washed with 70% ethanol. Purified circular RNAs were reverse transcribed with Rmrp- or 7SL-specific reverse primers (Supplemental Table 3) and SuperScript III. One tenth of cDNAs were further amplified with appropriate Rmrp- or 7SL-specific cRACE-forward and -reverse primers (Supplemental Table 3) and AccuPrime GC-rich DNA Polymerase (Invitrogen) to generated chimeric PCR products corresponding to 5′ and 3′ ends of related transcripts (Figure 3A). These PCR products were separated on 2% agarose gel and the bands of correct sizes were gel-extracted, purified and used in library preparation for MiSeq analysis using TruSeq Stranded

mRNA Sample Preparation Kits (Illumina). In order to perform Sanger sequencing analysis of cRACE products, before size selection on agarose gel, reactions were treated with Taq polymerase (Invitrogen) for 20 minutes at 72 °C. This incorporated an “A” overhang to PCR product and made them suitable for TA-cloning in pGEM-T easy vectors (Promega). Positive clones were analyzed by Sanger sequencing to identify 3′ ends of Rmrp and 7SL.

3′ end ligation RACE

After RNA isolation of FLAG-mutant Dis3l2 IP samples, 100 ng RNAs were ligated overnight at 25 °C to 2 μM Universal miRNA Cloning Linker (NEB) using 200 units of T4 RNA ligase 2 truncated KQ (NEB) at the presence of 25% PEG 8000, and RNaseOUT. Ligated RNAs were purified using RNA Clean & Concentrator-25 columns (Zymo Research) and reverse transcribed by SuperScript III (see RNA extraction and qRT-PCR section) and universal RT+linker primer (Supplemental Table 3). cDNAs were diluted and 100 ng cDNA was used for PCR reaction using U1 and U2 gene-specific forward primers (Supplemental Table 3) and universal RT+linker reverse primer. PCR products were gel-extracted and cloned into pGEM-T easy vectors (Promega) and sequenced by Sanger sequencing.

Statistics

All the experiments were performed for at least three times. For quantitative data, mean values ± standard error of means (SEM) were plotted. Student’s t-tests were used to analyze the significance of difference between different groups.

Supplementary Material

Refer to Web version on PubMed Central for supplementary material.

Acknowledgments

We thank Robinson Triboulet and Sager Gosai for helpful discussions, and Shuibin Lin for recombinant Zcchc11. This work was supported by grants to R.I.G. from the US National Institute of General Medical Sciences (NIGMS) (R01GM086386) and the March of Dimes Foundation (#1-FY15-3339).

References

Allison DS, Hall BD. Effects of alterations in the 3′ flanking sequence on in vivo and in vitro expression of the yeast SUP4-o tRNATyr gene. EMBO J. 1985; 4:2657–2664. [PubMed: 3902472]

Arimbasseri AG, Maraia RJ. Mechanism of Transcription Termination by RNA Polymerase III Utilizes a Non-template Strand Sequence-Specific Signal Element. Mol Cell. 2015; 58:1124–1132. [PubMed: 25959395]

Astuti D, Morris MR, Cooper WN, Staals RH, Wake NC, Fews GA, Gill H, Gentle D, Shuib S, Ricketts CJ, et al. Germline mutations in DIS3L2 cause the Perlman syndrome of overgrowth and Wilms tumor susceptibility. Nat Genet. 2012; 44:277–284. [PubMed: 22306653]

Bogenhagen DF, Brown DD. Nucleotide sequences in Xenopus 5S DNA required for transcription termination. Cell. 1981; 24:261–270. [PubMed: 6263489]

Bonafe L, Dermitzakis ET, Unger S, Greenberg CR, Campos-Xavier BA, Zankl A, Ucla C, Antonarakis SE, Superti-Furga A, Reymond A. Evolutionary comparison provides evidence for pathogenicity of RMRP mutations. PLoS Genet. 2005; 1:e47. [PubMed: 16244706]

Braglia P, Percudani R, Dieci G. Sequence context effects on oligo(dT) termination signal recognition by Saccharomyces cerevisiae RNA polymerase III. J Biol Chem. 2005; 280:19551–19562. [PubMed: 15788403]

Cai T, Aulds J, Gill T, Cerio M, Schmitt ME. The Saccharomyces cerevisiae RNase mitochondrial RNA processing is critical for cell cycle progression at the end of mitosis. Genetics. 2002; 161:1029–1042. [PubMed: 12136008]

Chang HM, Triboulet R, Thornton JE, Gregory RI. A role for the Perlman syndrome exonuclease Dis3l2 in the Lin28-let-7 pathway. Nature. 2013; 497:244–248. [PubMed: 23594738]

Cherkaoui Jaouad I, Laarabi FZ, Chafai Elalaoui S, Lyonnet S, Henrion-Caude A, Sefiani A. Novel Mutation and Structural RNA Analysis of the Noncoding RNase MRP Gene in Cartilage-Hair Hypoplasia. Mol Syndromol. 2015; 6:77–82. [PubMed: 26279652]

Chu S, Archer RH, Zengel JM, Lindahl L. The RNA of RNase MRP is required for normal processing of ribosomal RNA. Proc Natl Acad Sci U S A. 1994; 91:659–663. [PubMed: 8290578]

Dez C, Houseley J, Tollervey D. Surveillance of nuclear-restricted pre-ribosomes within a subnucleolar region of Saccharomyces cerevisiae. EMBO J. 2006; 25:1534–1546. [PubMed: 16541108]

Dieci G, Fiorino G, Castelnuovo M, Teichmann M, Pagano A. The expanding RNA polymerase III transcriptome. Trends Genet. 2007; 23:614–622. [PubMed: 17977614]

Faehnle CR, Walleshauser J, Joshua-Tor L. Mechanism of Dis3l2 substrate recognition in the Lin28-let-7 pathway. Nature. 2014; 514:252–256. [PubMed: 25119025]

Fagerlund RD, Perederina A, Berezin I, Krasilnikov AS. Footprinting analysis of interactions between the largest eukaryotic RNase P/MRP protein Pop1 and RNase P/MRP RNA components. RNA. 2015; 21:1591–1605. [PubMed: 26135751]

Garneau NL, Wilusz J, Wilusz CJ. The highways and byways of mRNA decay. Nat Rev Mol Cell Biol. 2007; 8:113–126. [PubMed: 17245413]

Gill T, Cai T, Aulds J, Wierzbicki S, Schmitt ME. RNase MRP cleaves the CLB2 mRNA to promote cell cycle progression: novel method of mRNA degradation. Mol Cell Biol. 2004; 24:945–953. [PubMed: 14729943]

Gold HA, Topper JN, Clayton DA, Craft J. The RNA processing enzyme RNase MRP is identical to the Th RNP and related to RNase P. Science. 1989; 245:1377–1380. [PubMed: 2476849]

Goldfarb KC, Cech TR. 3′ terminal diversity of MRP RNA and other human noncoding RNAs revealed by deep sequencing. BMC Mol Biol. 2013; 14:23. [PubMed: 24053768]

Haack TB, Kopajtich R, Freisinger P, Wieland T, Rorbach J, Nicholls TJ, Baruffini E, Walther A, Danhauser K, Zimmermann FA, et al. ELAC2 mutations cause a mitochondrial RNA processing defect associated with hypertrophic cardiomyopathy. Am J Hum Genet. 2013; 93:211–223. [PubMed: 23849775]

Haas G, Cetin S, Messmer M, Chane-Woon-Ming B, Terenzi O, Chicher J, Kuhn L, Hammann P, Pfeffer S. Identification of factors involved in target RNA-directed microRNA degradation. Nucleic Acids Res. 2016; 44:2873–2887. [PubMed: 26809675]

Hagan JP, Piskounova E, Gregory RI. Lin28 recruits the TUTase Zcchc11 to inhibit let-7 maturation in mouse embryonic stem cells. Nat Struct Mol Biol. 2009; 16:1021–1025. [PubMed: 19713958]

Heo I, Joo C, Kim YK, Ha M, Yoon MJ, Cho J, Yeom KH, Han J, Kim VN. TUT4 in concert with Lin28 suppresses microRNA biogenesis through pre-microRNA uridylation. Cell. 2009; 138:696–708. [PubMed: 19703396]

Hopper AK, Huang HY. Quality Control Pathways for Nucleus-Encoded Eukaryotic tRNA Biosynthesis and Subcellular Trafficking. Mol Cell Biol. 2015; 35:2052–2058. [PubMed: 25848089]

Hsieh CL, Donlon TA, Darras BT, Chang DD, Topper JN, Clayton DA, Francke U. The gene for the RNA component of the mitochondrial RNA-processing endoribonuclease is located on human chromosome 9p and on mouse chromosome 4. Genomics. 1990; 6:540–544. [PubMed: 2328993]

Huang W, Thomas B, Flynn RA, Gavzy SJ, Wu L, Kim SV, Hall JA, Miraldi ER, Ng CP, Rigo FW, et al. DDX5 and its associated lncRNA Rmrp modulate TH17 cell effector functions. Nature. 2015; 528:517–522. [PubMed: 26675721]

Ishikawa H, Nobe Y, Izumikawa K, Yoshikawa H, Miyazawa N, Terukina G, Kurokawa N, Taoka M, Yamauchi Y, Nakayama H, et al. Identification of truncated forms of U1 snRNA reveals a novel

RNA degradation pathway during snRNP biogenesis. Nucleic Acids Res. 2014; 42:2708–2724. [PubMed: 24311566]

Jacobson MR, Cao LG, Wang YL, Pederson T. Dynamic localization of RNase MRP RNA in the nucleolus observed by fluorescent RNA cytochemistry in living cells. J Cell Biol. 1995; 131:1649–1658. [PubMed: 8557735]

Kadaba S, Wang X, Anderson JT. Nuclear RNA surveillance in Saccharomyces cerevisiae: Trf4p-dependent polyadenylation of nascent hypomethylated tRNA and an aberrant form of 5S rRNA. RNA. 2006; 12:508–521. [PubMed: 16431988]

Kapusta A, Feschotte C. Volatile evolution of long noncoding RNA repertoires: mechanisms and biological implications. Trends Genet. 2014; 30:439–452. [PubMed: 25218058]

Kruger K, Grabowski PJ, Zaug AJ, Sands J, Gottschling DE, Cech TR. Self-splicing RNA: autoexcision and autocyclization of the ribosomal RNA intervening sequence of Tetrahymena. Cell. 1982; 31:147–157. [PubMed: 6297745]

LaCava J, Houseley J, Saveanu C, Petfalski E, Thompson E, Jacquier A, Tollervey D. RNA degradation by the exosome is promoted by a nuclear polyadenylation complex. Cell. 2005; 121:713–724. [PubMed: 15935758]

LaRiviere FJ, Cole SE, Ferullo DJ, Moore MJ. A late-acting quality control process for mature eukaryotic rRNAs. Mol Cell. 2006; 24:619–626. [PubMed: 17188037]

Leung E, Schneider C, Yan F, Mohi-El-Din H, Kudla G, Tuck A, Wlotzka W, Doronina VA, Bartley R, Watkins NJ, et al. Integrity of SRP RNA is ensured by La and the nuclear RNA quality control machinery. Nucleic Acids Res. 2014; 42:10698–10710. [PubMed: 25159613]

Lim J, Ha M, Chang H, Kwon SC, Simanshu DK, Patel DJ, Kim VN. Uridylation by TUT4 and TUT7 marks mRNA for degradation. Cell. 2014; 159:1365–1376. [PubMed: 25480299]

Lin S, Gregory RI. Identification of small molecule inhibitors of Zcchc11 TUTase activity. RNA Biol. 2015; 12:792–800. [PubMed: 26114892]

Lubas M, Damgaard CK, Tomecki R, Cysewski D, Jensen TH, Dziembowski A. Exonuclease hDIS3L2 specifies an exosome-independent 3′-5′ degradation pathway of human cytoplasmic mRNA. EMBO J. 2013; 32:1855–1868. [PubMed: 23756462]

Lygerou Z, Mitchell P, Petfalski E, Seraphin B, Tollervey D. The POP1 gene encodes a protein component common to the RNase MRP and RNase P ribonucleoproteins. Genes Dev. 1994; 8:1423–1433. [PubMed: 7926742]

Makitie O. Cartilage-hair hypoplasia in Finland: epidemiological and genetic aspects of 107 patients. J Med Genet. 1992; 29:652–655. [PubMed: 1404295]

Makitie O, Pukkala E, Teppo L, Kaitila I. Increased incidence of cancer in patients with cartilage-hair hypoplasia. J Pediatr. 1999; 134:315–318. [PubMed: 10064668]

Makitie OM, Tapanainen PJ, Dunkel L, Siimes MA. Impaired spermatogenesis: an unrecognized feature of cartilage-hair hypoplasia. Ann Med. 2001; 33:201–205. [PubMed: 11370774]

Maraia RJ, Lamichhane TN. 3′ processing of eukaryotic precursor tRNAs. Wiley Interdiscip Rev RNA. 2011; 2:362–375. [PubMed: 21572561]

Martin FH, Tinoco I Jr. DNA-RNA hybrid duplexes containing oligo(dA:rU) sequences are exceptionally unstable and may facilitate termination of transcription. Nucleic Acids Res. 1980; 8:2295–2299. [PubMed: 6159577]

Matsuzaki H, Kassavetis GA, Geiduschek EP. Analysis of RNA chain elongation and termination by Saccharomyces cerevisiae RNA polymerase III. J Mol Biol. 1994; 235:1173–1192. [PubMed: 8308883]

Mattick JS. The central role of RNA in human development and cognition. FEBS Lett. 2011; 585:1600–1616. [PubMed: 21557942]

Morris MR, Astuti D, Maher ER. Perlman syndrome: overgrowth, Wilms tumor predisposition and DIS3L2. Am J Med Genet C Semin Med Genet. 2013; 163:106–113. [PubMed: 23613427]

Nielsen S, Yuzenkova Y, Zenkin N. Mechanism of eukaryotic RNA polymerase III transcription termination. Science. 2013; 340:1577–1580. [PubMed: 23812715]

Orioli A, Pascali C, Pagano A, Teichmann M, Dieci G. RNA polymerase III transcription control elements: themes and variations. Gene. 2012; 493:185–194. [PubMed: 21712079]

Orioli A, Pascali C, Quartararo J, Diebel KW, Praz V, Romascano D, Percudani R, van Dyk LF, Hernandez N, Teichmann M, et al. Widespread occurrence of non-canonical transcription termination by human RNA polymerase III. Nucleic Acids Res. 2011; 39:5499–5512. [PubMed: 21421562]

Pirouz M, Rahjouei A, Shamsi F, Eckermann KN, Salinas-Riester G, Pommerenke C, Kessel M. Destabilization of pluripotency in the absence of Mad2l2. Cell Cycle. 2015; 14:1596–1610. [PubMed: 25928475]

Ridanpaa M, van Eenennaam H, Pelin K, Chadwick R, Johnson C, Yuan B, vanVenrooij W, Pruijn G, Salmela R, Rockas S, et al. Mutations in the RNA component of RNase MRP cause a pleiotropic human disease, cartilage-hair hypoplasia. Cell. 2001; 104:195–203. [PubMed: 11207361]

Rinn JL, Chang HY. Genome regulation by long noncoding RNAs. Annu Rev Biochem. 2012; 81:145–166. [PubMed: 22663078]

Shukla S, Parker R. Quality control of assembly-defective U1 snRNAs by decapping and 5′-to-3′ exonucleolytic digestion. Proc Natl Acad Sci U S A. 2014; 111:E3277–3286. [PubMed: 25071210]

Slevin MK, Meaux S, Welch JD, Bigler R, Miliani de Marval PL, Su W, Rhoads RE, Prins JF, Marzluff WF. Deep sequencing shows multiple oligouridylations are required for 3′ to 5′ degradation of histone mRNAs on polyribosomes. Mol Cell. 2014; 53:1020–1030. [PubMed: 24656133]

Thiel CT, Mortier G, Kaitila I, Reis A, Rauch A. Type and level of RMRP functional impairment predicts phenotype in the cartilage hair hypoplasia-anauxetic dysplasia spectrum. Am J Hum Genet. 2007; 81:519–529. [PubMed: 17701897]

Thomas MP, Liu X, Whangbo J, McCrossan G, Sanborn KB, Basar E, Walch M, Lieberman J. Apoptosis Triggers Specific, Rapid, and Global mRNA Decay with 3′ Uridylated Intermediates Degraded by DIS3L2. Cell Rep. 2015; 11:1079–1089. [PubMed: 25959823]

Thornton JE, Chang HM, Piskounova E, Gregory RI. Lin28-mediated control of let-7 microRNA expression by alternative TUTases Zcchc11 (TUT4) and Zcchc6 (TUT7). RNA. 2012; 18:1875–1885. [PubMed: 22898984]

Trojak JE, Polmar SH, Winkelstein JA, Hsu S, Francomano C, Pierce GF, Scillian JJ, Gale AN, McKusick VA. Immunologic studies of cartilage-hair hypoplasia in the Amish. Johns Hopkins Med J. 1981; 148:157–164. [PubMed: 6970848]

Ustianenko D, Hrossova D, Potesil D, Chalupnikova K, Hrazdilova K, Pachernik J, Cetkovska K, Uldrijan S, Zdrahal Z, Vanacova S. Mammalian DIS3L2 exoribonuclease targets the uridylated precursors of let-7 miRNAs. RNA. 2013; 19:1632–1638. [PubMed: 24141620]

Vanacova S, Wolf J, Martin G, Blank D, Dettwiler S, Friedlein A, Langen H, Keith G, Keller W. A new yeast poly(A) polymerase complex involved in RNA quality control. PLoS Biol. 2005; 3:e189. [PubMed: 15828860]

Wegert J, Ishaque N, Vardapour R, Georg C, Gu Z, Bieg M, Ziegler B, Bausenwein S, Nourkami N, Ludwig N, et al. Mutations in the SIX1/2 pathway and the DROSHA/DGCR8 miRNA microprocessor complex underlie high-risk blastemal type Wilms tumors. Cancer Cell. 2015; 27:298–311. [PubMed: 25670083]

Wolin SL, Sim S, Chen X. Nuclear noncoding RNA surveillance: is the end in sight? Trends Genet. 2012; 28:306–313. [PubMed: 22475369]

HIGHLIGHTS

- Dis3l2 selectively regulates noncoding RNAs including Rmrp, 7SL, and snRNAs
- Zcchc6 and Zcchc11 are TUTases responsible for noncoding RNA uridylation
- Dis3l2-TUTase axis recognizes and degrades aberrant Rmrp species
- Dis3l2-Mediated Decay (DMD) is a noncoding RNA quality control pathway

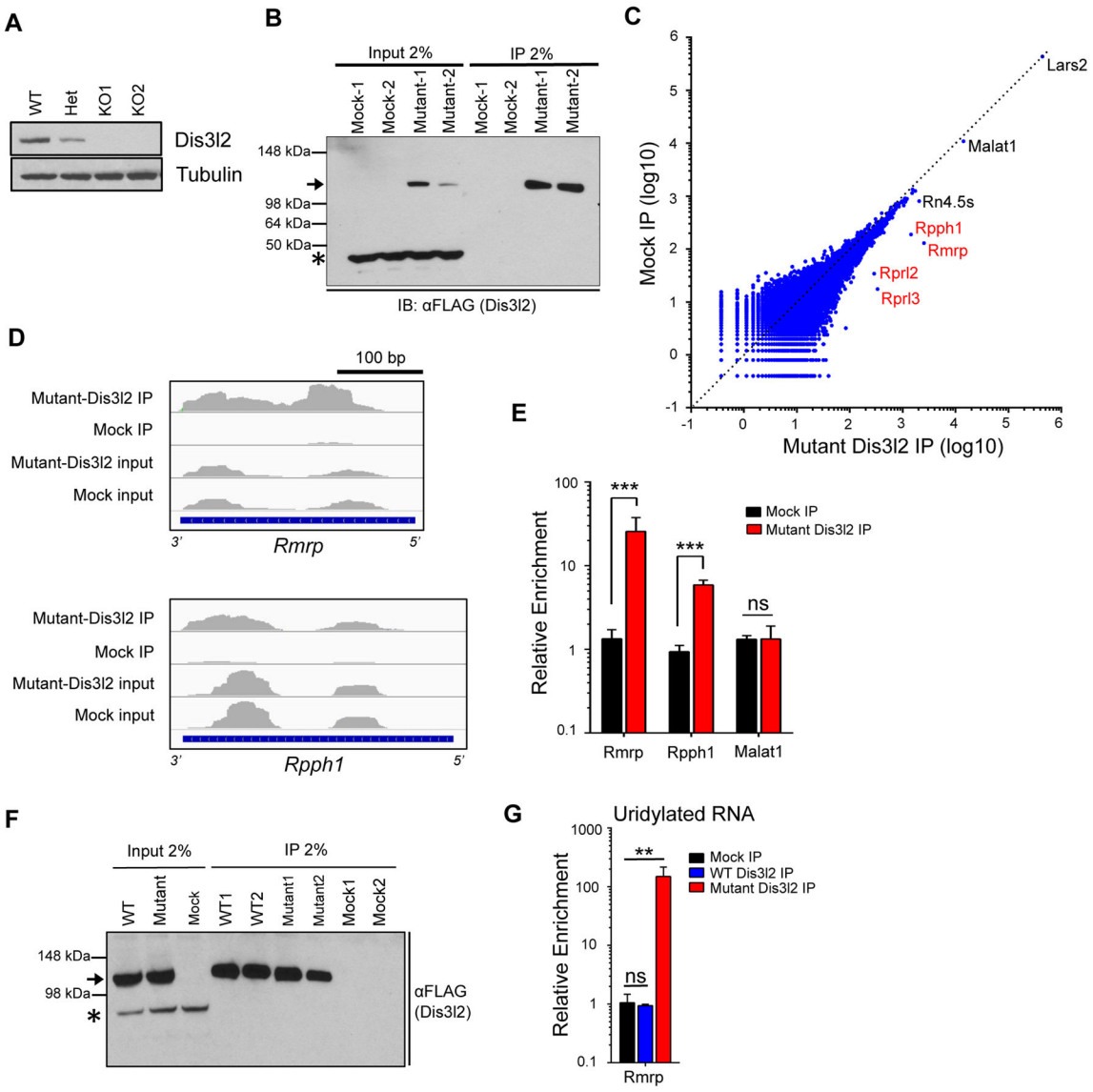

Figure 1. Systematic identification of Dis3l2-associated RNAs in mouse ESCs

(A) Western blot analysis of Dis3l2 expression in CRISPR-Cas9 generated knockout ESCs; WT, wild type; Het, heterozygous; KO, knockout. **(B)** Western blot analysis of FLAG-tagged Dis3l2 in input and IP samples. Arrow points to the FLAG-mutant Dis3l2 expression in knockout ESCs (Inputs) and after anti-FLAG immunoprecipitation (IPs). Asterisk shows an unspecific band, representing equal loading. Empty pFLAG-CMV2 vector was used as mock. **(C)** Scatter plotting of enriched transcripts in FLAG-mutant Dis3l2 IP compared to Mock IP. Among the most enriched transcripts are Rmrp, Rpph1, and the two Rpph1 pseudogenes, Rprl2 and Rprl3, all highlighted in red. **(D)** Representative sequencing track of Rmrp and Rpph1 in inputs and IPs. Read numbers range from 0–3500. **(E)** qRT-PCR analysis of FLAG-immunoprecipitated RNAs (n=6). Note that Malat1 was not enriched in FLAG-mutant Dis3l2 IP. To measure relative enrichment of each gene, expressions in IP samples were first normalized to Gapdh level and then to the respective input; ns, not

significant. **F)** Anti-FLAG immunoblotting of Dis3l2 knockout cellular lysates after overexpression of WT, mutant Dis3l2, or mock transfected cells as well as related immunoprecipitation. **(G)** qRT-PCR analysis of FLAG-immunoprecipitated RNAs. Oligo-dA primers were used for cDNA synthesis after RNA-IP to measure relative uridylation levels (n=6); ns, not significant. Where related, bars represent mean ± SEM. **$p \leq 0.01$, ***$p \leq 0.001$, Student's t-test. See also Supplemental Figure 1 and Supplemental Table 1.

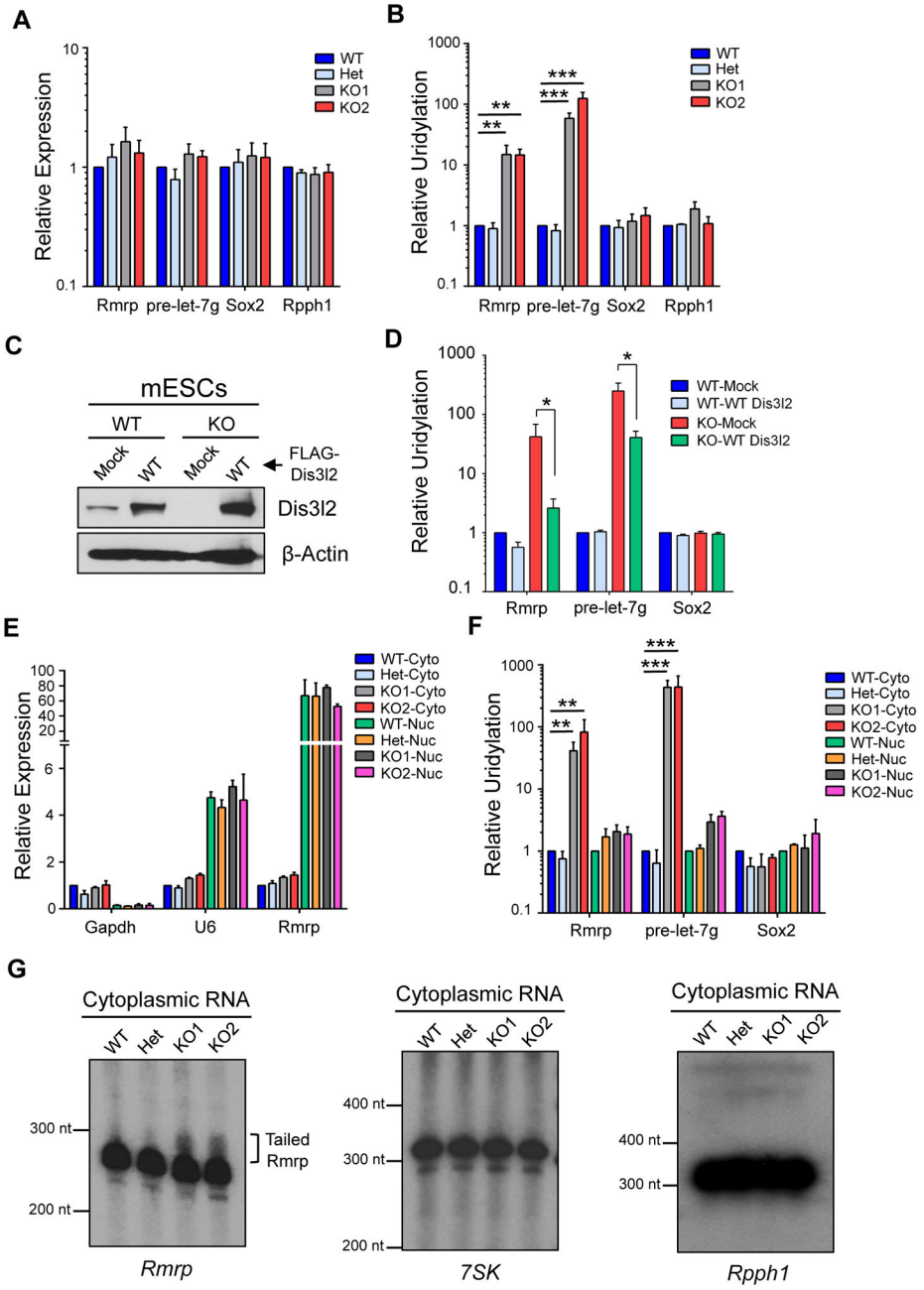

Figure 2. Uridylated Rmrp transcripts accumulate in the cytoplasm of Dis3l2 deficient ESCs

(A) qRT-PCR analysis of total gene expression in Dis3l2 knockout ESCs (n=4). **(B)** Increased relative uridylation of Rmrp and pre-let7g, but not Rpph1 or Sox2 in Dis3l2-depleted ESCs (n=4). **(C)** Anti-Dis3l2 western blotting of wild type and knockout ESCs, transiently transfected with mock or wild type Dis3l2 expressing vectors. **(D)** Wild type Dis3l2 re-expression in knockout cells significantly decreased the uridylated Rmrp and pre-let-7g transcripts, but not Sox2 (n=3). **(E)** qRT-PCR confirmation of cytoplasmic (Cyto) and nuclear (Nuc) fractionation of ESCs (n=4). **(F)** Increased relative uridylation of Rmrp and pre-let-7g in the cytoplasm of Dis3l2 deficient ESCs, but not in nuclear fractions (n=4). **(G)**

Northern blot analysis of cytoplasmic RNAs in ESCs. Note to the slowly migrating species representing tailed Rmrp. No such tailed 7SK or Rpph1 transcripts were observed in cytoplasmic fraction of Dis3l2 knockout ESCs. Where related, bars represent mean ± SEM. *p ≤ 0.05, **p ≤ 0.01, ***p ≤ 0.001, ****p ≤ 0.0001, Student's t-test. See also Supplemental Figure 2.

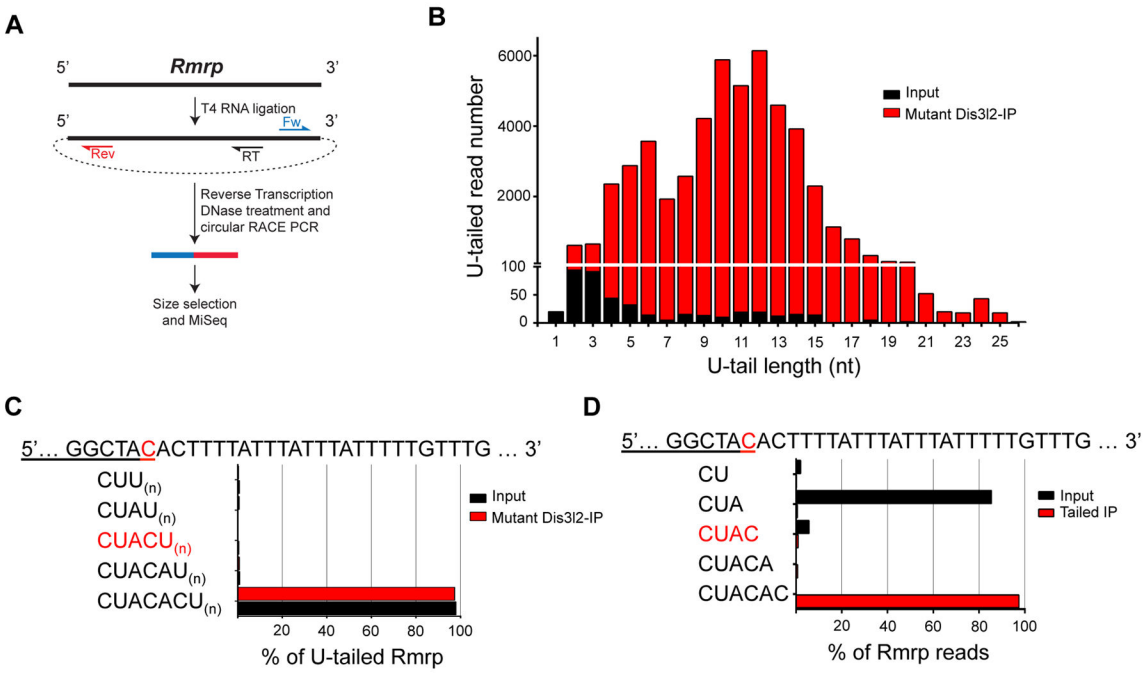

Figure 3. Deep sequencing analysis of the 3′-end of Rmrp RNA

(A) Schematic protocol for Rmrp cRACE. See the method section for details. **(B)** The distribution and length of U-tails in input and FLAG-mutant Dis3l2-IP RNAs. Note the 10–12 nucleotide-long peak in the U-tail length in the Dis3l2-bound Rmrp reads. **(C)** Analysis of Rmrp 3′ end revealed that U-tails are mainly added to transcripts with 2 additional nucleotides at their 3′ compared to annotated gene. **(D)** In input samples, majority of Rmrp species are terminated 1 nucleotide before the annotated transcript (highlighted in red), while the U-tailed Rmrp reads in IP samples always end 2 nucleotides downstream.

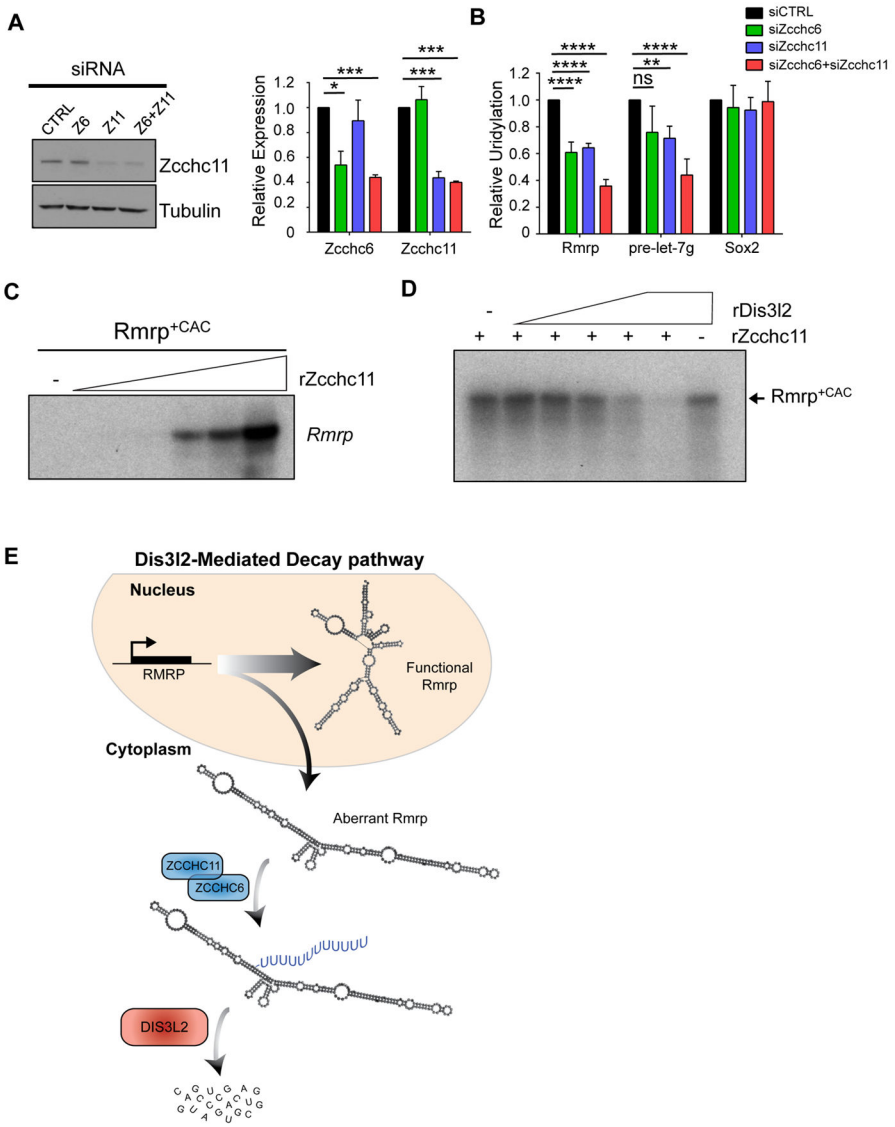

Figure 4. TUTase-dependent Dis3l2-mediated decay of Rmrp

(A) Western blot (left panel) and qRT-PCR analyses confirmed the knockdown of two TUTases, Zcchc6 and Zcchc11 in Dis3l2 knockout ESCs (n=3). **(B)** Individual and combinatorial knockdown of TUTases alleviates relative uridylation of Rmrp and pre-let-7g in Dis3l2 knockout ESCs (n=3). **(C)** In vitro uridylation assay using recombinant Zcchc11 (rZcchc11). In vitro transcribed Rmrp^{+CAC} was incubated with radiolabeled UTP and increasing amounts of rZcchc11. Reactions were run on TBE-Urea gels and visualized by autoradiography. **(D)** In vitro reconstitution of TUTase-dependent Dis3l2-dependent Rmrp decay. In vitro transcribed radiolabeled Rmrp^{+CAC} was incubated with a buffer containing rUTP and, where indicated, rZcchc11 and increasing amounts of recombinant Dis3l2 (rDis3l2). **(E)** A model representing the function of TUTase-Dis3l2 axis in degradation of aberrant Rmrp. Based on this Dis3l2-mediated decay pathway model, mutant Rmrp transcripts are exported to the cytoplasm, where they are further uridylated by TUTases,

Zcchc6 and Zcchc11, and subsequently degraded by Dis3l2 to eliminate these nonfunctional species.

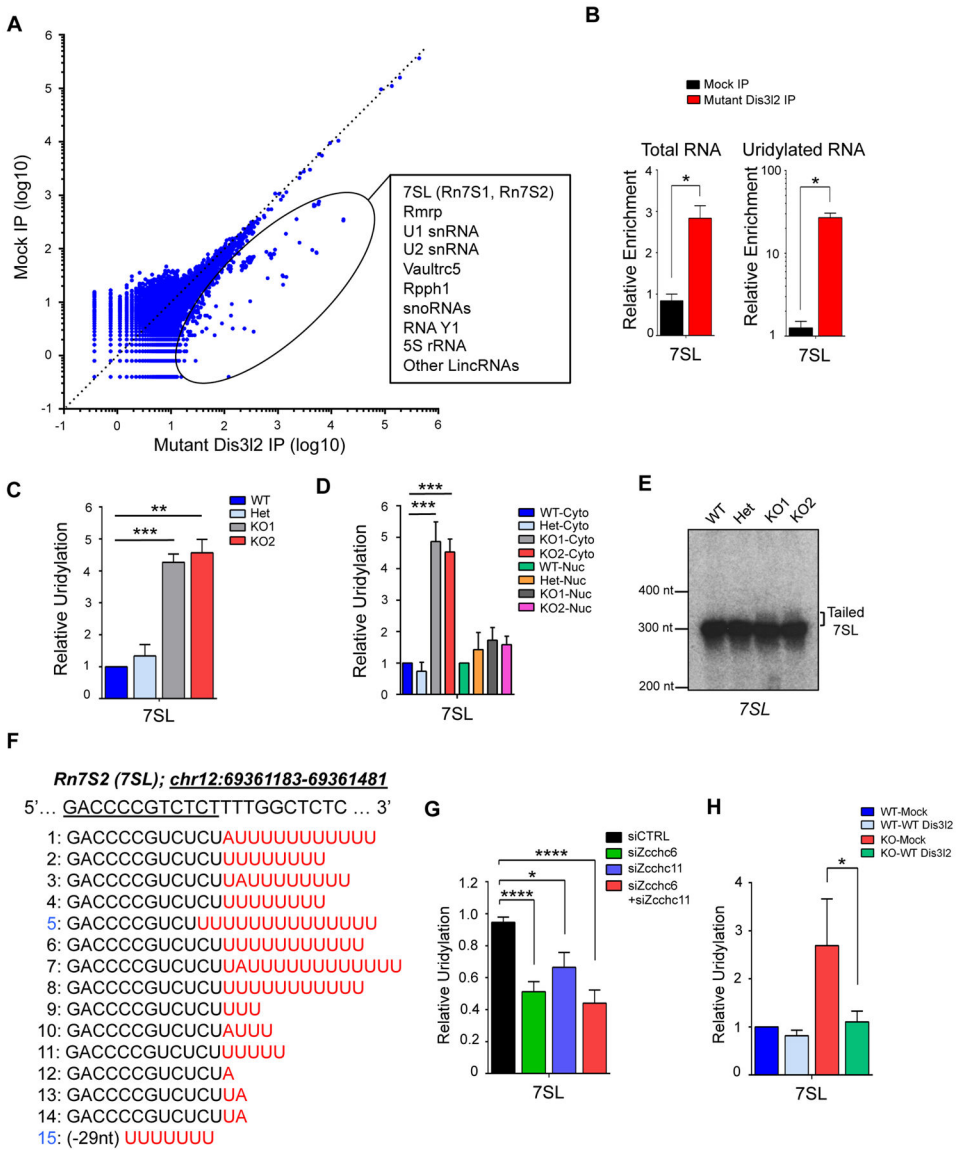

Figure 5. Systematic analysis of Dis3l2-bound noncoding RNAs

(A) Scatter plot of enriched ncRNA transcripts in FLAG-mutant Dis3l2 IP compared to Mock IP. cDNA libraries from Figure 1C were aligned to noncoding genome (see methods section). **(B)** qRT-PCR analysis of total and uridylated 7SL immunoprecipitated by FLAG-mutant Dis3l2 (n=3). Increased relative uridylation of 7SL in total cell lysates **(C)** (n=3) and in cytoplasmic fractions **(D)** of Dis3l2 deficient ESCs. **(E)** Northern blot analysis of 7SL in ESCs. Note the slowly migrating species in RNA samples from Dis3l2-deficient ESCs. **(F)** cRACE analysis of 7SL tails in FLAG-mutant Dis3l2 immunoprecipitated RNA samples. Sanger sequencing analysis revealed U-tails of different length in several clones (shown in red). In some clones, the U-tail occurred after 3′-end truncated species (clones 5 and 15, marked in blue). **(G)** qRT-PCR revealed that Zcchc6 and Zcchc11 knockdown reduces relative uridylation of 7SL (n=3). **(H)** qRT-PCR showed that re-expression of Dis3l2 rescues the elevated uridylation of 7SL transcripts in Dis3l2 knockout cells (n=3). Bars represent

mean ± SEM. *p ≤ 0.05, **p ≤ 0.01, ***p ≤ 0.001, ****p ≤ 0.0001, Student's t-test. See also Supplemental Figure 4 and Supplemental Table 1 and 2.

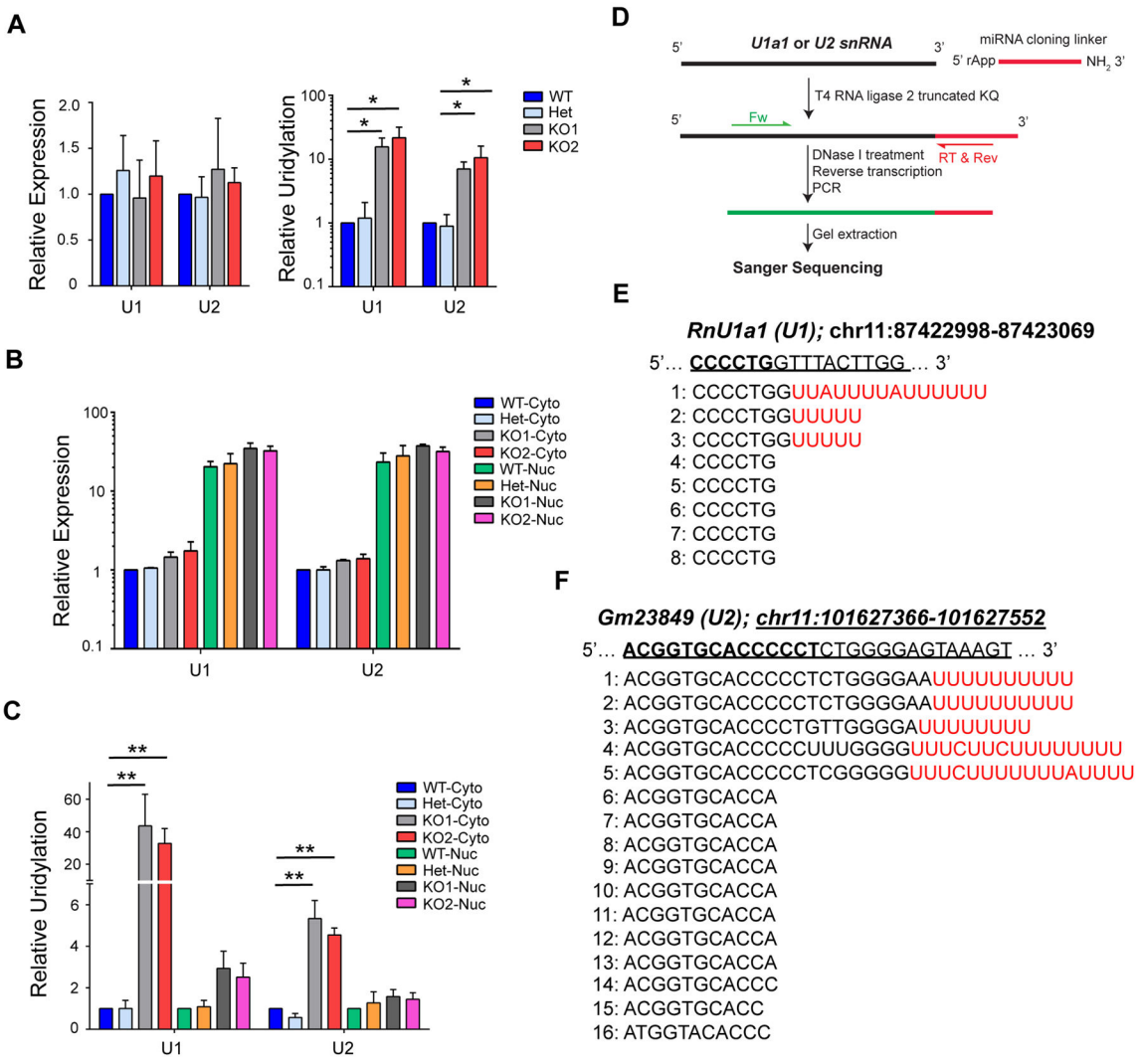

Figure 6. Dis3l2 targets uridylated U1 and U2 snRNAs

(A) Relative expression (left panel) and relative uridylation (right panel) of U1 (U1-a1) and U2 (U2–10) snRNAs in Dis3l2-depleted ESCs. **(B)** Cellular fractionation and qRT-PCR analysis confirming nuclear disctribution of U1 and U2. **(C)** Increased uridylation levels of U1 and U2 in cytoplasmic fractions of Dis3l2 knockout cells. **(D)** Schematic representation of 3′ end-ligation RACE protcol established for U1 and U2 snRNAs. **(E, F)** Sanger sequencing analysis of 3′-ligation RACE PCR products from FLAG-Mutant Dis3l2-bound RNAs revealed frequent clones with non-genomic U-rich tails in U1 **(E)** and U2 **(F)** snRNA species. For A–C, bars represent mean ± SEM. (n=3) *p ≤ 0.05, **p ≤ 0.01, Student's t-test. See also Supplemental Table 2.